

# Enhanced Antiferromagnetic Phase in Metastable Self-Intercalated $\text{Cr}_{1+x}\text{Te}_2$ Compounds

Clayton Conner,<sup>1</sup> Ali Sarikhani,<sup>2</sup> Theo Volz,<sup>3</sup> Mitchel Vaninger,<sup>1</sup> Xiaoqing He,<sup>4</sup>  
Steven Kelley,<sup>5</sup> Jacob Cook,<sup>1</sup> Avinash Sah,<sup>1</sup> John Clark,<sup>1</sup> Hunter Lucker,<sup>1</sup> Cheng  
Zhang,<sup>1</sup> Paul Miceli,<sup>1</sup> Yew San Hor,<sup>2</sup> Xiaoqian Zhang,<sup>6</sup> and Guang Bian<sup>1,7</sup>

<sup>1</sup>*Department of Physics and Astronomy,  
University of Missouri, Columbia, Missouri 65211, USA*

<sup>2</sup>*Department of Physics and Astronomy,  
Missouri University of Science and Technology, Rolla, Missouri 65409, USA*

<sup>3</sup>*Rock Bridge High School, Columbia, Missouri 65203, USA*

<sup>4</sup>*Electron Microscopy Core Facility,  
University of Missouri, Columbia, Missouri 65211, USA*

<sup>5</sup>*Department of Chemistry, University of Missouri, Columbia, Missouri 65211, USA*

<sup>6</sup>*Key Laboratory of Quantum Materials and Devices of Ministry of Education,  
School of Physics, Southeast University, Nanjing 211189, China*

<sup>7</sup>*MU Materials Science & Engineering Institute,  
University of Missouri, Columbia, MO, 65211, USA*

## Abstract

Magnetic transition-metal dichalcogenides (TMDs) have been of particular interest due to their unique magnetic properties and layered structure that can be promising for a wide range of spintronic applications. One of the most exciting compounds in this family of magnets is chromium telluride,  $\text{Cr}_{1+x}\text{Te}_2$ , which has shown rich magnetic phases with varied Cr concentrations. An emergent antiferromagnetic (AFM) ordering has been found in  $\text{Cr}_{1.25}\text{Te}_2$  (equivalently,  $\text{Cr}_5\text{Te}_8$ ), which is induced by intercalating 0.25 Cr atom per unit cell within the van der Waals (vdW) gaps of  $\text{CrTe}_2$ . In this work, we report an increased Néel Temperature ( $T_N$ ) of the AFM phase in  $\text{Cr}_{1+x}\text{Te}_2$  by slightly reducing the concentration of Cr intercalants. Moreover, the intercalated Cr atoms form a metastable  $2\times 2$  supercell structure that can be manipulated by electron beam irradiation. This work offers a promising approach to tuning magnetic and structural properties by adjusting the concentration of self-intercalated magnetic atoms.

## I. INTRODUCTION

2D magnetic materials have become an intense focus of research in the field of condensed matter physics due to their unique properties and practical applications to the field of spintronics. Transition-metal dichalcogenides (TMDs) are layered structures with van der Waals (vdW) gaps between subsequent atomic layers. TMDs have been heavily researched in the past because of this two-dimensional layered vdW structure. This provides the ability to produce atomically thin films with various desired characteristics [1]. Recently, vdW magnetic materials have become an area of emphasis in novel magnetism owing to their relative ease of production, thickness-dependent magnetic properties, and persistence of magnetic ordering down to the two-dimensional regime [2, 3]. Materials such as  $\text{Cr}_2\text{Ge}_2\text{Te}_6$  [4],  $\text{Fe}_3\text{GeTe}_2$  [5, 6], and  $\text{CrI}_3$  [7] have all been heavily studied and show magnetic ordering that persists in the two-dimensional limit; however, many of these materials have a Curie Temperature ( $T_C$ ) much lower than room temperature, making them largely impractical for device applications. Among the known vdW materials, one of the most promising is the transition-metal dichalcogenide  $\text{CrTe}_2$ , which has been reported to have magnetic ordering down to one monolayer with a  $T_C$  close to room temperature [8].

Layered materials like TMDs also provide a very promising avenue for creating synthetic antiferromagnets. Antiferromagnetic (AFM) based devices can exhibit ultra-fast switching and produce large magnetotransport effects. These unique magnetic properties make AFM-type van der Waals (vdW) materials an exciting platform for spintronics research, as they generate no stray magnetic fields and are unaffected by disruptive magnetic fields from other devices [9]. Materials such as  $\text{CrBr}_3$  have a stacking dependence on their magnetic ordering, with different stacking ordering resulting in either an AFM or FM phase [10]. Similarly,  $\text{CrI}_3$  has been shown to have a giant tunneling magnetoresistance (MR) while also having an intrinsic AFM coupling between layers [11]. Despite the exciting promise of these layered materials, they often require complex fabrication and their transition temperatures are generally well below room temperature.

Magnetic TMDs contain van der Waals (vdW) gaps between subsequent layers that can be intercalated with transition metals, creating new compounds that maintain the layered, quasi-2D structure. These compounds can have unique properties that are quite different from the parent vdW material. This intercalation method can be utilized to tune desirable

magnetic properties for device applications[12, 13]. This tunability through intercalation has been well demonstrated in chromium telluride compounds, denoted as  $\text{Cr}_{1+x}\text{Te}_2$ . These compounds have the layered base structure of  $\text{CrTe}_2$ , belonging to the space group  $\text{P}\bar{3}\text{m}$  [14], in which Cr atoms can be intercalated within the vdW gaps between the  $\text{CrTe}_2$  layers, thus creating new compounds [15]. For example,  $x = 0$  ( $\text{CrTe}_2$ ), 0.25 ( $\text{Cr}_5\text{Te}_8$ ), 0.33 ( $\text{Cr}_2\text{Te}_3$ ), 0.50 ( $\text{Cr}_3\text{Te}_4$ ), and 1 ( $\text{CrTe}$ ). Due to the self-intercalation of Cr within the vdW gaps, the properties of these compounds differ from the pristine  $\text{CrTe}_2$  base compound. As a result, the family of  $\text{Cr}_{1+x}\text{Te}_2$  compounds in bulk show a variation of  $T_C$ , magnetic ordering, and even structural properties [16–18]. This wide range of properties necessitates a systematic study of how self-intercalation can be used to manipulate the properties of vdW compounds.

One of the intercalated variants,  $\text{Cr}_5\text{Te}_8$ , has been heavily studied and is ferromagnetic with a  $T_C$  of approximately 150 K in bulk. Other interesting magnetic properties of this compound such as colossal Anomalous Hall Effect [19] and thickness-dependent  $T_C$  [20] have been reported. In this work, we will focus on a reported emergent antiferromagnetic (AFM) phase in  $\text{Cr}_5\text{Te}_8$ , which demonstrates a large negative MR that enables effectively a spin valve device [21]. However, the sub-room-temperature Néel ( $T_N$ ) and Curie ( $T_C$ ) temperatures of  $\text{Cr}_5\text{Te}_8$  hinder practical device application of this compound. In this work, We explore the structural and magnetic behaviors of non-integer stoichiometries with  $x < 0.25$  in an effort to tune these properties for more suitable device conditions. Our experiments demonstrate that a slight reduction in Cr concentration from  $\text{Cr}_5\text{Te}_8$  leads to a metastable structure of intercalants and a dramatically increased  $T_N$ .

## II. RESULTS AND DISCUSSION

Single crystals of  $\text{Cr}_{1+x}\text{Te}_2$  of two different Cr concentrations ( $x = 0.223$  and  $x = 0.202$ ) were fabricated using the self-flux growth method. This is a slight reduction of Cr concentration from the  $\text{Cr}_5\text{Te}_8$  ( $x = 0.25$ ) compound, giving the stoichiometries of  $\text{Cr}_{4.89}\text{Te}_8$  and  $\text{Cr}_{4.81}\text{Te}_8$ , respectively. These single crystal samples serve as a platform for investigating the structural and magnetic effects through varying the concentration of intercalated Cr within the vdW gaps. X-ray diffraction (XRD) measurements reveal the formation of a monoclinic crystal structure belonging to the space group  $\text{I}2/\text{m}$ . These compounds share a similar structure to  $\text{Cr}_5\text{Te}_8$  with self-intercalated atoms within the vdW gap of the  $\text{CrTe}_2$  base layers;

however, these compounds contain two inequivalent Cr sites with partial occupancy located within the vdW gap. These Cr sites are labeled as  $Cr_4$  and  $Cr_7$  in Figure 1(a), with the  $Cr_4$  site having a higher statistical occupancy than the  $Cr_7$  site (Table 1). In this context, statistical occupancy refers to the probability of finding either intercalated Cr atom located at its respective site. The monoclinic  $Cr_5Te_8$  crystal structure, on the other hand, contains one fully occupied Cr site located between the  $CrTe_2$  layers. These  $Cr_4$  and  $Cr_7$  intercalated sites create a  $2 \times 2$  periodicity along in-plane directions due to the inequivalent occupancy of the sites. The lattice constants were determined using single crystal XRD for both compounds, respectively, as shown in Table 1. We can directly compare these measured lattice constants to the reported monoclinic  $Cr_5Te_8$  structure of  $a = 13.575 \text{ \AA}$ ,  $b = 7.859 \text{ \AA}$ , and  $c = 12.073 \text{ \AA}$ [22]. While  $a$  and  $b$  are almost unchanged,  $c$  show a reduction of 0.77% and 0.93% for  $Cr_{1+x}Te_2$  ( $x = 0.223, 0.202$ ), respectively. This is due to the reduced concentration of Cr intercalants. As the  $c$  lattice parameter reflects the coupling between  $CrTe_2$  layers, the result suggests an increase in interlayer coupling compared to that of  $Cr_5Te_8$ .

Transmission Electron Microscopy (TEM) and Scanning Transmission Electron Microscopy (STEM) were used to fully characterize the structure of these  $Cr_{1+x}Te_2$  samples. Figure 1(c) shows a cross-sectional TEM measurement of  $Cr_{4.89}Te_8$  along the (010) direction, confirming the layered quasi 2D structure consistent with the XRD results. High-angle annular dark-field (HAADF)-STEM was performed on this sample, and the result is shown in Figure 1(b). The overlaid XRD structure (marked by the yellow and blue balls) aligns well with the HAADF-STEM measurements. An out-of-plane (OOP) TEM image of the lattice can be seen in Figure 1(e), which is in good agreement with XRD results (Figure 1(d)). The high structural quality of this compound is further confirmed by the selected area electron diffraction (SAED) measurement. The corresponding hexagonal periodicity (Figure 1(f)) of the SAED result is indexed according to the XRD structure.

Fast Fourier Transform (FFT) was applied to the cross-sectional TEM image to show the periodicity of the lattice along the (010) direction (Figure 2). This FFT result exhibited the expected periodicity and high degree of crystallinity as indicated by the bright spots (Figure 2a). The FFT image was then indexed according to the XRD crystal structure, as noted in the figure. In addition to the expected periodicity, a second periodicity can be seen as indicated by the dimmer spots (highlighted by the yellow circles). Those spots are located closer to the (000) peak, indicative of a superstructure in real space. This

superstructure in reciprocal space has a  $2\times 2$  periodicity that matches exactly with the  $2\times 2$  periodicity of the intercalated Cr sites,  $\text{Cr}_4$  and  $\text{Cr}_7$ , as shown in the structure above the FFT image in Figure 2(a). Interestingly, the metastability of this superstructure was observed during the TEM measurements. After exposure to the electron beam from TEM, the  $2\times 2$  superstructure spots begin to fade in brightness, as seen in Figure 2(b). After several minutes under electron beam irradiation, the superstructure disappears completely (Figure 2(c)). This effect implies that the  $\text{Cr}_4$  and  $\text{Cr}_7$  sites have much lower binding energy than the Cr atoms in the  $\text{CrTe}_2$  main layer. The scattering with the electron beam provides Cr intercalants enough energy to overcome the binding energy, allowing the Cr intercalants to move randomly within the van der Waals gap and destroy the superstructure periodicity, as schematically depicted in Figs. 2(b,c). Turning off the electron beam, the superstructure is restored after several minutes as shown in Figure 2(d), indicating the metastability of the  $2\times 2$  superstructure of Cr intercalants.

The effects of altering the concentration of Cr intercalants were studied by the measurements of magnetic properties of the  $\text{Cr}_{1+x}\text{Te}_2$  compounds. The magnetic hysteresis loops at various temperatures (10–300K) for the  $\text{Cr}_{4.89}\text{Te}_8$  and  $\text{Cr}_{4.81}\text{Te}_8$  compounds can be seen in Figure 3(a-d). Neither compound fully saturates under an in-plane (IP) magnetic field even up to a field strength of 6 Tesla (Figs. 3(a,c)). In contrast, the OOP field measurement on both  $\text{Cr}_{4.89}\text{Te}_8$  and  $\text{Cr}_{4.81}\text{Te}_8$  compounds show the magnetization fully saturates at approximately the same value under a much lower field strength than the IP measurement (Figs. 3(b,d)). This confirms a large perpendicular magnetic anisotropy (PMA), an essential ingredient for stabilizing ferromagnetism in 2D materials[23], and an out-of-plane magnetic easy axis in both compounds. This behavior can be attributed to the parallel exchange coupling within the  $\text{CrTe}_2$  layers. It is interesting to note that both  $\text{Cr}_{4.89}\text{Te}_8$  and  $\text{Cr}_{4.81}\text{Te}_8$  compounds have negligible coercivity, even at very low temperatures, consistent with the typical small coercivity value previously found in  $\text{Cr}_5\text{Te}_8$  [8, 24].

The temperature-dependent magnetization,  $M(T)$  of the two self-intercalated compounds was measured using a superconducting quantum interference device (SQUID) at various magnetic field strengths over a temperature range from 50 K to 300 K. Figures 4( a,b) show the OOP field measurement of the  $\text{Cr}_{4.89}\text{Te}_8$  and  $\text{Cr}_{4.81}\text{Te}_8$  compounds, with both compounds exhibiting the characteristic ferromagnetic behavior with the magnetization increasing suddenly as the temperature is reduced below the  $T_c$ . In addition to the ferromagnetic transition,

we observed the appearance of a subtle cusp-like feature at 180 K and 240 K for  $\text{Cr}_{4.89}\text{Te}_8$  and  $\text{Cr}_{4.81}\text{Te}_8$ , respectively. As mentioned previously, a similar cusp-like feature has been previously reported as an AFM transition in  $\text{Cr}_5\text{Te}_8$  [21], but the AFM phase transition is much more prominent in the OOP  $M(T)$  measurements of  $\text{Cr}_5\text{Te}_8$ . The in-plane field measurements on the two compounds exhibit a similar FM behavior in the magnetization but with a much lower magnitude than the OOP magnetization, indicating an OOP easy axis of magnetization. On the other hand, the IP  $M(T)$  curves exhibit a more pronounced cusp-like feature, resembling the AFM phase transition previously observed in  $\text{Cr}_5\text{Te}_8$ . This is especially apparent for the  $\text{Cr}_{4.89}\text{Te}_8$  compound shown in Figure 4(d), which shows this cusp-like feature occurs at 241 K. The  $\text{Cr}_{4.81}\text{Te}_8$  material also exhibits a cusp-like feature in the IP  $M(T)$  curve (Figure 4(e)), but at a lower temperature of 222 K. The  $M(T)$  result indicates that slightly reducing the concentration of Cr intercalants leads to a similar AFM phase as that of  $\text{Cr}_5\text{Te}_8$  but with an IP antiparallel spin ordering.

The effects of reducing Cr concentration on the Curie and Néel temperatures of these compounds are fully characterized by examining the  $M(T)$  curves. The derivative of the magnetization with respect to temperature,  $dM/dT$ , was taken to determine the values of  $T_C$  and  $T_N$ . Figure 4(c) shows the  $dM/dT$  results for both  $\text{Cr}_{4.89}\text{Te}_8$  and  $\text{Cr}_{4.81}\text{Te}_8$  compounds in a temperature range of 140-240 K with an OOP field strength of 100 Oe. Due to the clear ferromagnetic behavior measured in the out-of-plane direction, we can directly extract the  $T_C$  from the  $dM/dT$  curves. A sharp negative peak can be seen for both compounds, the peak location corresponding to the  $T_C$  of these two materials. The ferromagnetic transition peaks of both compounds overlap one another, giving the Curie temperature of 163 K for both compounds. This is approximately 15 K higher than the  $T_C$  of the  $\text{Cr}_5\text{Te}_8$  compound found in the previous work, but both  $\text{Cr}_{4.89}\text{Te}_8$  and  $\text{Cr}_{4.81}\text{Te}_8$  share the same Curie temperature despite the slightly different Cr concentration. This increase in  $T_C$  suggests that a decrease in Cr concentration from  $\text{Cr}_5\text{Te}_8$  increases the ferromagnetic stability. This result can be explained by the fact that the reduction of intercalated Cr leads to a smaller vertical lattice constant  $c$ , enhances interlayer exchange coupling, and pushes the system closer to the base compound of  $\text{CrTe}_2$ , which is known to have a room-temperature  $T_C$ . The signature of the emergent AFM phase in  $\text{Cr}_5\text{Te}_8$  is a cusp-like feature in the magnetization-temperature  $M(T)$  curve appearing at a temperature about  $T_C$ . This is because the appearance of antiparallel spin ordering alters the slope of the  $M(T)$  curve. With an OOP field, the AFM-induced slope

change in  $M(T)$  occurs around 185 K and 220 K for  $\text{Cr}_{4.89}\text{Te}_8$  and  $\text{Cr}_{4.81}\text{Te}_8$ , respectively. However, this cusp-like feature is less prominent than that of  $\text{Cr}_5\text{Te}_8$  in the OOP field (Figs. 4(a-c)). By contrast, a more prominent cusp-like feature was observed in the  $M(T)$  curves of  $\text{Cr}_{4.89}\text{Te}_8$  and  $\text{Cr}_{4.81}\text{Te}_8$  measured with an IP magnetic field (Figs. 4(d-f)), indicating that the antiparallel magnetic ordering tends to align in the IP direction. The  $T_N$  of these compounds can be extracted by applying the same  $dM/dT$  method to the IP  $M(T)$  data. The  $T_N$  of these compounds can be calculated this way because the AFM ordering creates a change in the slope of the  $M(T)$  curves. As shown in Figure 4(f), the emergent AFM peaks appear at temperatures higher than  $T_C$ . Unlike the  $T_C$  peaks, these peaks occur at different temperatures for the two compounds. The  $T_N$  of  $\text{Cr}_{4.89}\text{Te}_8$  is measured to be at 241 K at 150 Oe IP field strength, which is a very dramatic increase of approximately 60 K from the  $T_N$  found in the  $\text{Cr}_5\text{Te}_8$  compound. The AFM peak of  $\text{Cr}_{4.81}\text{Te}_8$  occurs at 222K, lower than the  $\text{Cr}_{4.89}\text{Te}_8$  compound. Nevertheless, this is still around a 40 K increase from the  $T_N$  of  $\text{Cr}_5\text{Te}_8$ . While still not reaching the desired room temperature, the elevated  $T_N$  caused by adjusting Cr concentration is a significant stride towards the practical applications of the emergent AFM ordering and the related spin valve function in these vdW magnets [21].

The observed enhancement of the AFM ordering indicates an interesting relation between the concentration of self-intercalation and Néel temperature. The decrease of the intercalated Cr creates an increase in the  $T_N$  and causes an emergent in-plane AFM ordering despite the out-of-plane ferromagnetic ground state. The origin of this in-plane AFM phase can be attributed to several potential mechanisms. One possible mechanism for the in-plane nature of the antiferromagnetic ordering is the existence of a helical AFM state [25]. The coexistence of ferromagnetic and antiferromagnetic phases in different directions has been observed in systems that exhibit this helical AFM ordering [26]. In addition, the structural effect on the magnetic properties of these compounds must be considered. A trend of decreasing  $c$  lattice parameter with the reduction of intercalated Cr has been confirmed by our XRD results. This  $c$  lattice parameter directly reflects the interlayer distance between the  $\text{CrTe}_2$  base layers. This reduction of the interlayer spacing can lead to a stronger hybridization between the  $3d$  orbitals of Cr and the  $5p$  orbitals of Te, thus enhancing the superexchange coupling. The superexchange coupling is highly dependent on the bond distances and angles associated with the Cr-Te-Cr paths to make it either AFM or FM type [27, 28]. Another mechanism that should be considered in this context is the



Ruderman-Kittel-Kasuya-Yosida (RKKY) coupling, which is a very important component in the formation of synthetic antiferromagnetic materials such as  $\text{Cr}_5\text{Te}_8$  [29]. In the RKKY model, interlayer magnetic coupling between ferromagnetic layers oscillates with respect to the thickness of a nonmagnetic spacer between layers [30, 31]. The intercalated Cr atoms in this system can also behave as the nonmagnetic spacer between the magnetically ordered  $\text{CrTe}_2$  layers. By tuning this nonmagnetic layer thickness, we can then tune the interlayer magnetic coupling, leading to changes in magnetic behavior and ordering. The interlayer spacing associated with the  $\text{Cr}_{4.89}\text{Te}_8$  seemingly provides an ideal spacing for the antiparallel alignment of the moments in  $\text{CrTe}_2$  layers. Further reducing Cr concentration leads to a reduction in  $T_N$  due to this oscillatory behavior in interlayer exchange coupling as a function of interlayer spacing. A very similar behavior was observed in Co-doped  $\text{Fe}_4\text{GeTe}_2$  vdW magnets [32], where variation in the Co concentration led to a controllable  $T_N$  and changes direction of the Néel vector. Further research is needed to elucidate the significant increase in  $T_N$  and the IP nature of the AFM phase observed in the  $\text{Cr}_{1+x}\text{Te}_8$  compounds.

One of the most intriguing properties found in the  $\text{Cr}_5\text{Te}_8$  compound was the large negative magnetoresistance (MR) that occurred between the  $T_C$  and  $T_N$ . This effect can be attributed to the coexistence of the FM and AFM phases, creating a single-crystal MR spin valve device that can be controlled by very small fields. Therefore, it is important to explore the effects of the reduced Cr concentration on this MR behavior. As shown in Figure 5(a), we measure the longitudinal resistance with varied OOP magnetic fields for the  $\text{Cr}_{4.81}\text{Te}_8$  compound. It can be seen that the measured MR decreases at larger fields due to the alignment of magnetic moments. Zooming in on the MR curves, it's clear that a bump feature appears in the MR curves around the zero field in a temperature window of 170–200 K and is fully suppressed above 220 K. The bump in MR curves is due to the enhancement of electron scattering with antiparallel magnetic texture in the AFM phase. The temperature window in which the enhanced MR appears coincides with the temperature range between  $T_C$  (165 K) and  $T_N$  (220 K) of  $\text{Cr}_{4.81}\text{Te}_8$  in an OOP field, confirming the emergent AFM ordering in the ferromagnetic compound.

Based on our measurements, we construct a plot showing the variation in magnetic properties of the  $\text{Cr}_{1+x}\text{Te}_2$  compounds including the  $\text{Cr}_{4.89}\text{Te}_8$  and  $\text{Cr}_{4.81}\text{Te}_8$  compounds, as shown in Figure 5(b). This picture shows how magnetic properties can be tuned by varying the intercalant concentration. Starting with  $\text{CrTe}_2$  ( $X=0$ ), we have the largest measured

Curie temperature of the group and the robustness of maintaining this high  $T_C$  down to the 2D limit. With the increase of Cr concentration, we arrive at the materials discussed in this work ( $\text{Cr}_{4.81}\text{Te}_8$ ,  $\text{Cr}_{4.89}\text{Te}_8$ ,  $\text{Cr}_5\text{Te}_8$ ) that exhibit an emergent AFM phase in addition to ferromagnetic ground state, with  $\text{Cr}_{4.89}\text{Te}_8$  having the highest  $T_N$ . Finally, a further increase in Cr produces  $\text{Cr}_2\text{Te}_3$ , which has a higher  $T_C$  than the materials in this work[17], but lacks the AFM phase.

### III. CONCLUSION

In this work, we demonstrate structural and magnetic properties of two self-intercalated  $\text{Cr}_{1+x}\text{Te}_2$  ( $x = 0.223, 0.202$ ) compounds with slightly reduced concentration of Cr intercalants compared to that of  $\text{Cr}_5\text{Te}_8$  ( $x = 0.25$ ). A  $2 \times 2$  metastable superstructure of partially occupied intercalated Cr sites was observed in those compounds that could be manipulated by electron beam irradiation in a completely reversible process. Despite having different Cr concentrations, both compounds show the same Curie temperature of 165 K, which is 10 K higher than that of  $\text{Cr}_5\text{Te}_8$ . Remarkably, both compounds exhibit an emergent AFM phase, as previously reported in  $\text{Cr}_5\text{Te}_8$ . However, unlike  $\text{Cr}_5\text{Te}_8$ , this AFM ordering appears in the in-plane direction. In addition, we see a prominent increase in Néel temperature of these self-intercalated compounds, as the  $T_N$  of  $\text{Cr}_{4.89}\text{Te}_8$  is 241 K. This work demonstrates that varying intercalant concentration offers a practical route to tuning the magnetic and structural properties of vdW magnets for spintronic applications.

### IV. METHODS

#### A. Growth of $\text{Cr}_{1+x}\text{Te}_2$ ( $x = 0.223, 0.202$ ) compounds

The  $\text{Cr}_{1+x}\text{Te}_2$  samples were produced using a chemical vapor transport (CVT) method, which involves a two-step process to create large single crystals. High-purity chromium (Cr, 99.99%) powder and tellurium (Te, 99.999%) lumps were sourced from Alfa Aesar for this growth process. Initially, a stoichiometrically correct mixture of Cr and Te was prepared and placed into a fused quartz ampule, repetitively cleaned with ultra-high-purity (UHP) argon, and sealed under a high vacuum. These ampules were heated to 950°C for 24 hours, then cooled at a rate of 1°C per minute to room temperature. The polycrystalline product

was then ground into a fine, smooth powder using an agate mortar and pestle, creating a precursor ready for CVT growth.

For the CVT growth, 1 gram of the prepared powdered precursor was placed into a 30 cm-long quartz ampule with a 12 mm inner diameter, along with 3 mg of high-purity iodine pieces per  $\text{cm}^3$  of internal ampule volume, which serves as the transport agent. The ampules were sealed under the same vacuum and argon conditions as the precursor preparation. To achieve a temperature gradient essential for CVT, a three-zone Thermo Scientific Lindberg Blue M furnace was used. First, zones 2 and 3 of the furnace were preheated to  $950^\circ\text{C}$  while zone 1 was maintained at  $650^\circ\text{C}$  for 24 hours to eliminate any impurities on the quartz surface. Following this cleaning phase, the zones were adjusted to 950, 600, and  $850^\circ\text{C}$  respectively, establishing a temperature gradient for efficient vapor transport, with thermocouple readouts recorded as 950, 808, and  $850^\circ\text{C}$ , respectively. This configuration was held steady for two months for a thermal equilibrium as well as larger crystal growth. After the growth phase, the temperature across all zones was gradually equalized to  $650^\circ\text{C}$  and then reduced to room temperature at a rate of  $1^\circ\text{C}$  per minute. Large crystals were cleaved and selected from the bulk for characterization and measurement.

## **B. Transmission Electron Microscopy and HAADF-STEM**

Lamellar samples were removed from bulk  $\text{Cr}_{1+x}\text{Te}_2$  crystals using FIB milling by a FEI Scios DualBeam SEM. TEM and HAADF-STEM images were obtained using a ThermoScientific Spectra 300 electron microscope.

## **C. Transport and Magnetic Measurements**

Magnetic characterization was performed using a Quantum Design superconducting quantum interference device (SQUID). This device has a base temperature of 2 K and a magnetic field of up to 7 T. The magnetoresistance measurements were performed on a Quantum Design Physical Property Measurement System (PPMS) with a base temperature of 2 K and magnetic field up to 9 T. The devices were confined to the Hall-bar geometry using a stan-

standard four-point probe method with room-temperature cured silver paste contacts.

---

- [1] W. Choi, N. Choudhary, G. H. Han, J. Park, D. Akinwande, and Y. H. Lee, *Materials Today* **20**, 116 (2017).
- [2] Y. Khan, S. M. Obaidulla, M. R. Habib, A. Gayen, T. Liang, X. Wang, and M. Xu, *Nano Today* **34**, 100902 (2020).
- [3] K. S. Burch, D. Mandrus, and J.-G. Park, *Nature* **563**, 47 (2018).
- [4] C. Gong, L. Li, Z. Li, H. Ji, A. Stern, Y. Xia, T. Cao, W. Bao, C. Wang, Y. Wang, Z. Q. Qiu, R. J. Cava, S. G. Louie, J. Xia, and X. Zhang, *Nature* **546**, 265 (2017).
- [5] H. L. Zhuang, P. R. C. Kent, and R. G. Hennig, *Phys. Rev. B* **93**, 134407 (2016).
- [6] J.-X. Zhu, M. Janoschek, D. S. Chaves, J. C. Cezar, T. Durakiewicz, F. Ronning, Y. Sassa, M. Mansson, B. L. Scott, N. Wakeham, E. D. Bauer, and J. D. Thompson, *Phys. Rev. B* **93**, 144404 (2016).
- [7] B. Huang, G. Clark, E. Navarro-Moratalla, D. R. Klein, R. Cheng, K. L. Seyler, D. Zhong, E. Schmidgall, M. A. McGuire, D. H. Cobden, W. Yao, D. Xiao, P. Jarillo-Herrero, and X. Xu, *Nature* **546**, 270 (2017).
- [8] X. Zhang, Q. Lu, W. Liu, W. Niu, J. Sun, J. Cook, M. Vaninger, P. F. Miceli, D. J. Singh, S.-W. Lian, T.-R. Chang, X. He, J. Du, L. He, R. Zhang, G. Bian, and Y. Xu, *Nature Communications* **12**, 2492 (2021).
- [9] V. Baltz, A. Manchon, M. Tsoi, T. Moriyama, T. Ono, and Y. Tserkovnyak, *Rev. Mod. Phys.* **90**, 015005 (2018).
- [10] W. Chen, Z. Sun, Z. Wang, L. Gu, X. Xu, S. Wu, and C. Gao, *Science* **366**, 983 (2019), <https://www.science.org/doi/pdf/10.1126/science.aav1937>.
- [11] T. Song, X. Cai, M. W.-Y. Tu, X. Zhang, B. Huang, N. P. Wilson, K. L. Seyler, L. Zhu, T. Taniguchi, K. Watanabe, M. A. McGuire, D. H. Cobden, D. Xiao, W. Yao, and X. Xu, *Science* **360**, 1214 (2018), <https://www.science.org/doi/pdf/10.1126/science.aar4851>.
- [12] M. Rajapakse, B. Karki, U. O. Abu, S. Pishgar, M. R. K. Musa, S. M. S. Riyadh, M. Yu, G. Sumanasekera, and J. B. Jasinski, *npj 2D Materials and Applications* **5**, 30 (2021).
- [13] X. Zhao, P. Song, C. Wang, A. C. Riis-Jensen, W. Fu, Y. Deng, D. Wan, L. Kang, S. Ning, J. Dan, T. Venkatesan, Z. Liu, W. Zhou, K. S. Thygesen, X. Luo, S. J. Pennycook, and K. P.

- Loh, *Nature* **581**, 171 (2020).
- [14] L. Meng, Z. Zhou, M. Xu, S. Yang, K. Si, L. Liu, X. Wang, H. Jiang, B. Li, P. Qin, P. Zhang, J. Wang, Z. Liu, P. Tang, Y. Ye, W. Zhou, L. Bao, H.-J. Gao, and Y. Gong, *Nature Communications* **12**, 809 (2021).
- [15] Y. Fujisawa, M. Pardo-Almanza, J. Garland, K. Yamagami, X. Zhu, X. Chen, K. Araki, T. Takeda, M. Kobayashi, Y. Takeda, C. H. Hsu, F. C. Chuang, R. Laskowski, K. H. Khoo, A. Soumyanarayanan, and Y. Okada, *Phys. Rev. Mater.* **4**, 114001 (2020).
- [16] Y. Wang, J. Yan, J. Li, S. Wang, M. Song, J. Song, Z. Li, K. Chen, Y. Qin, L. Ling, H. Du, L. Cao, X. Luo, Y. Xiong, and Y. Sun, *Phys. Rev. B* **100**, 024434 (2019).
- [17] H. Ipsier, K. L. Komarek, and K. O. Klepp, *Journal of the Less Common Metals* **92**, 265 (1983).
- [18] J. Dijkstra, H. H. Weitering, C. F. van Bruggen, C. Haas, and R. A. de Groot, *Journal of Physics: Condensed Matter* **1**, 9141 (1989).
- [19] B. Tang, X. Wang, M. Han, X. Xu, Z. Zhang, C. Zhu, X. Cao, Y. Yang, Q. Fu, J. Yang, X. Li, W. Gao, J. Zhou, J. Lin, and Z. Liu, *Nature Electronics* **5**, 224 (2022).
- [20] C. Chen, X. Chen, C. Wu, X. Wang, Y. Ping, X. Wei, X. Zhou, J. Lu, L. Zhu, J. Zhou, T. Zhai, J. Han, and H. Xu, *Advanced Materials* **34**, 2107512 (2022), <https://onlinelibrary.wiley.com/doi/pdf/10.1002/adma.202107512>.
- [21] X. Zhang, W. Liu, W. Niu, Q. Lu, W. Wang, A. Sarikhani, X. Wu, C. Zhu, J. Sun, M. Vaninger, P. F. Miceli, J. Li, D. J. Singh, Y. S. Hor, Y. Zhao, C. Liu, L. He, R. Zhang, G. Bian, D. Yu, and Y. Xu, *Advanced Functional Materials* **32**, 2202977 (2022), <https://onlinelibrary.wiley.com/doi/pdf/10.1002/adfm.202202977>.
- [22] W. Bensch, O. Helmer, and C. Näther, *Materials Research Bulletin* **32**, 305 (1997).
- [23] M. Gibertini, M. Koperski, A. F. Morpurgo, and K. S. Novoselov, *Nature Nanotechnology* **14**, 408 (2019).
- [24] K. Lukoschus, S. Kraschinski, C. Näther, W. Bensch, and R. Kremer, *Journal of Solid State Chemistry* **177**, 951 (2004).
- [25] S. Kobayashi, *Phys. Rev. Lett.* **106**, 057207 (2011).
- [26] N. S. Sangeetha, V. Smetana, A.-V. Mudring, and D. C. Johnston, *Phys. Rev. B* **100**, 094438 (2019).
- [27] H. Y. Lv, W. J. Lu, D. F. Shao, Y. Liu, and Y. P. Sun, *Phys. Rev. B* **92**, 214419 (2015).

- [28] N. Sivadas, S. Okamoto, X. Xu, C. J. Fennie, and D. Xiao, *Nano Letters* **18**, 7658 (2018), pMID: 30408960, <https://doi.org/10.1021/acs.nanolett.8b03321>.
- [29] R. A. Duine, K.-J. Lee, S. S. P. Parkin, and M. D. Stiles, *Nature Physics* **14**, 217 (2018).
- [30] D. M. Edwards, J. Mathon, R. B. Muniz, and M. S. Phan, *Phys. Rev. Lett.* **67**, 493 (1991).
- [31] S. S. P. Parkin, N. More, and K. P. Roche, *Phys. Rev. Lett.* **64**, 2304 (1990).
- [32] J. Seo, E. S. An, T. Park, S.-Y. Hwang, G.-Y. Kim, K. Song, W.-S. Noh, J. Y. Kim, G. S. Choi, M. Choi, E. Oh, K. Watanabe, T. Taniguchi, J.-H. Park, Y. J. Jo, H. W. Yeom, S.-Y. Choi, J. H. Shim, and J. S. Kim, *Nature Communications* **12**, 2844 (2021).

## FIGURES

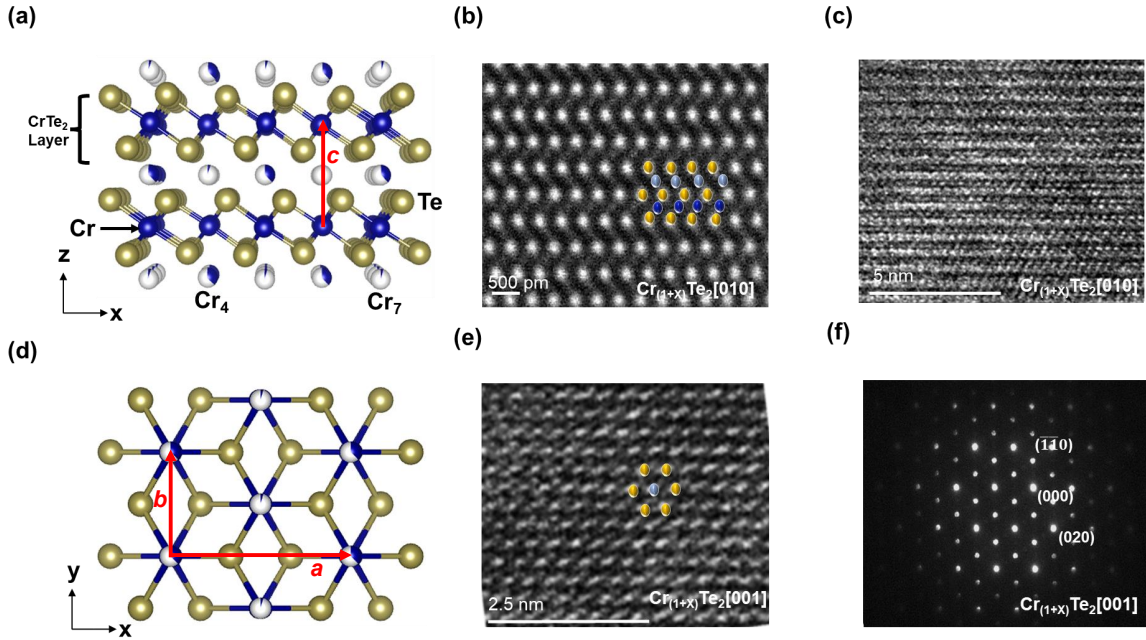


FIG. 1. (a) Crystal structure of  $\text{Cr}_{1+x}\text{Te}_2$  along the (010) direction with  $\text{Cr}_4$  and  $\text{Cr}_7$  intercalant sites intercalated within vdW gap between  $\text{CrTe}_2$  layers. A  $2 \times 2$  periodic superstructure can be seen from these intercalated sites. This structure is confirmed by XRD measurements. (b) HAADF-STEM image of  $\text{Cr}_{1+x}\text{Te}_2$  along the (010) direction. (c) Cross-sectional TEM image of  $\text{Cr}_{1+x}\text{Te}_2$  along the (010) direction, showing a quasi-2D layered structure that matches with the XRD data shown in (a). (d) Top view of the crystal structure along the (001) direction showing hexagonal structure. (e) The TEM image along the (001) direction that matches the structure shown in (d). (f) Electron diffraction pattern showing hexagonal periodicity that is indexed according to the XRD structure shown in (d).



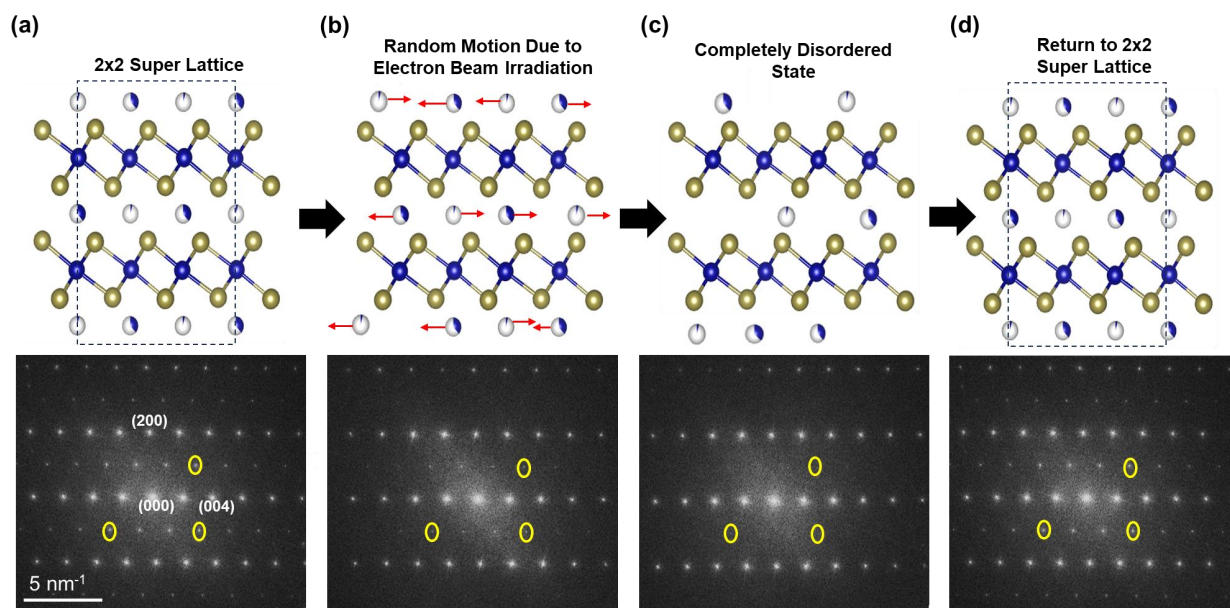


FIG. 2. (a) Side view of the crystal structure of  $\text{Cr}_{1+x}\text{Te}_2$  as determined by XRD (top panel) and fast Fourier transform (FFT) of the TEM image taken along the  $(010)$  direction (bottom panel). The spots highlighted by the yellow circles in the FFT measurement correspond to the  $2 \times 2$  superlattice periodicity of Cr intercalants. (b,c) Same as (a) but taken from samples after 2 and 10 minutes under electron beam irradiation in TEM. (d) The TEM image was taken from the sample after the electron beam was stopped for several minutes.

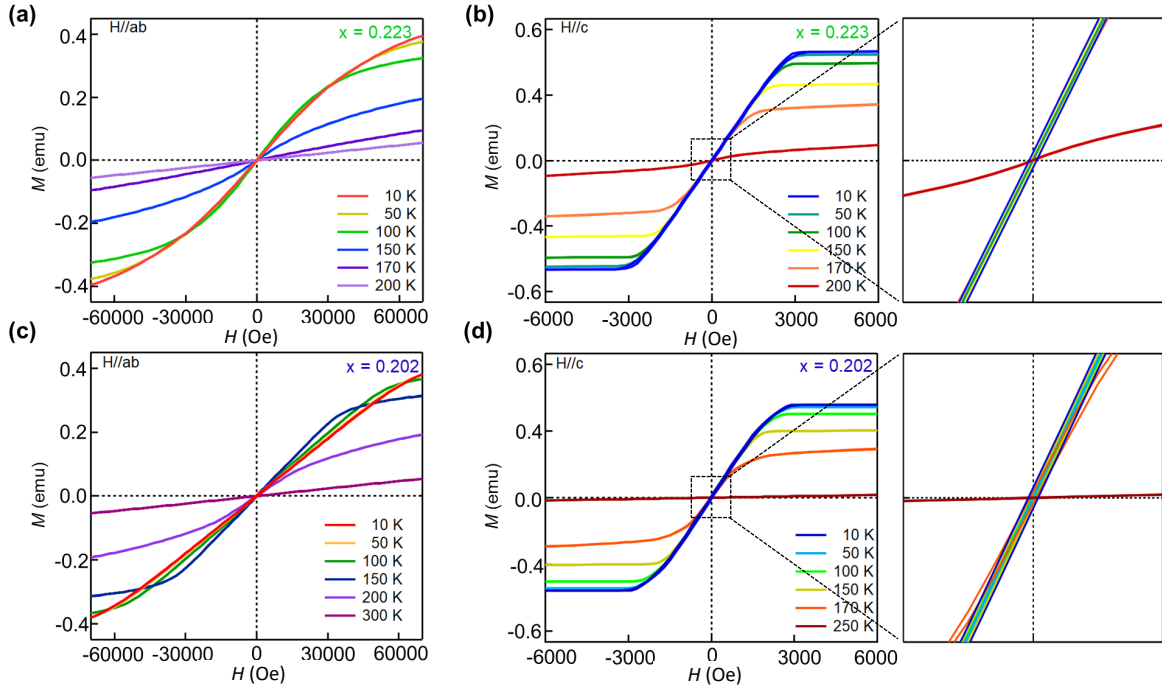


FIG. 3. (a) Magnetization of  $\text{Cr}_{4.89}\text{Te}_8$  as a function of the field strength of IP magnetic field measured at different temperatures. (b) Same as (a) but measured with OOP magnetic fields. The zoom-in in (b) shows a very small magnetic coercivity at different temperatures. (c,d) Same as (a,b) but for  $\text{Cr}_{4.81}\text{Te}_8$ .

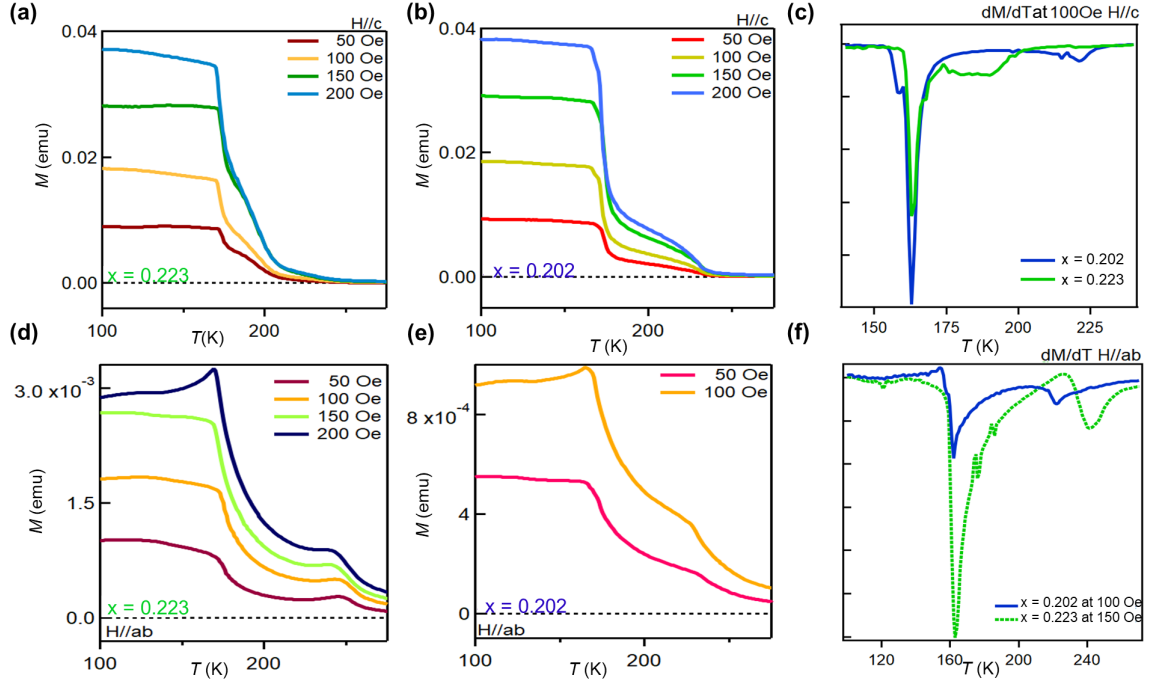


FIG. 4. (a, b) Magnetization measured with different OOP magnetic fields for  $\text{Cr}_{4.89}\text{Te}_8$  and  $\text{Cr}_{4.81}\text{Te}_8$ , respectively. (c) Temperature-derivative of magnetization,  $dM/dT$ , taken at the OOP field strength of 100 Oe for both compounds. (d-f) Same as (a-c) but measured with IP magnetic fields with field strength indicated in each panel.

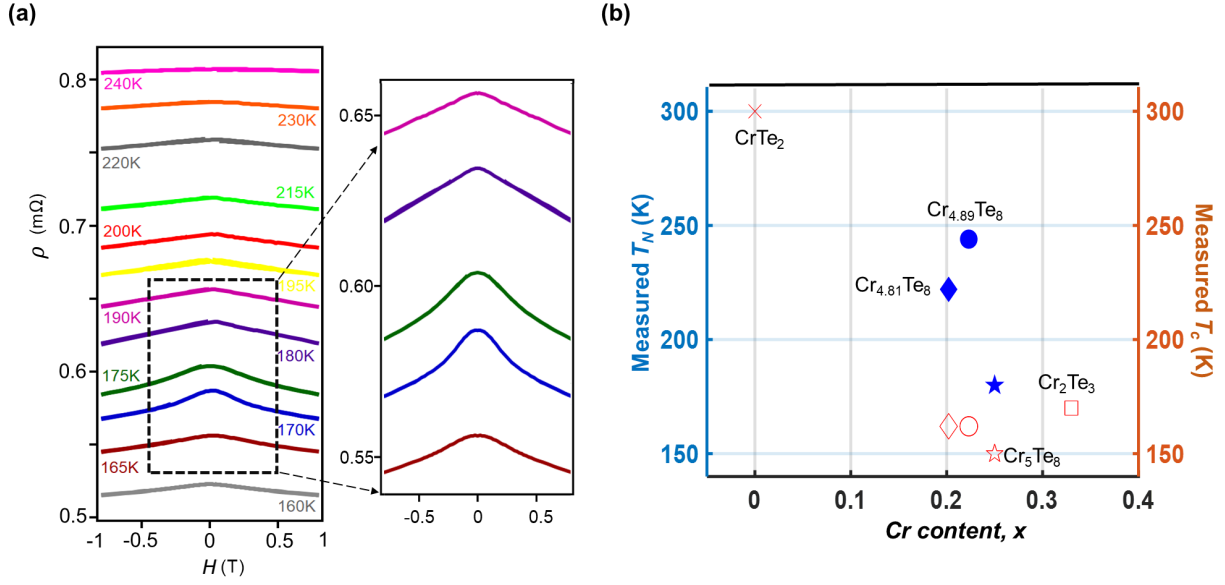


FIG. 5. (a) Measured longitudinal resistance of  $\text{Cr}_{4.81}\text{Te}_8$  as a function of the strength of OOP magnetic field measured at different temperatures. (b) Summary of reported  $T_C$  (red) and the  $T_N$  (blue) for the  $\text{Cr}_{1+x}\text{Te}_2$  compounds. The blue solid symbols mark the measured  $T_N$ , if applicable, while the red unfilled symbols for the measured  $T_C$ .

## TABLES

Measured Composition	$\text{Cr}_{(1+x)}\text{Te}_2$	Occupancy		Lattice Constants ( $\text{\AA}$ )		
	x Value	$\text{Cr}_4$	$\text{Cr}_7$	a	b	c
$\text{Cr}_{4.89}\text{Te}_8$	0.223	0.391	0.062	13.546	7.814	11.980
$\text{Cr}_{4.81}\text{Te}_8$	0.202	0.337	0.068	13.546	7.820	11.961

TABLE I. Chemical composition and lattice constants of the  $\text{Cr}_{1+x}\text{Te}_2$  samples measured by XRD.